第 6 卷 第 1 期 航空动力学报 Vol. 6 No. 1
1991 年 1 月 Journal of Aerospace Power Jan. 1991

高、低能扰动力函数对叶轮机阵发非定常气动力的影响

2-E FORCING FUNCTION EFFECTS ON TURBOMACHINE GUST UNSTEADY AERODYNAMICS

Steven R. Manwaring and Sanford Fleeter (*Purdue University*)

ABSTRACT To investigate the forcing function effects on the fundamental 2-E gust unsteady aerodynamic response of a multistage turbomachine blade row, a series of fundamental experiments are performed in an axial flow research compressor. The 2-E unsteady aerodynamic forcing function excitations are generated by both a circumferential inlet flow distortion and the wakes from airfoil-type obstructions which are representative of an airfoil, strut, or probe excitation.

【摘要】 为了研究扰动力函数对多级叶轮机叶片排中基本的高、低能阵发非定常气动响应的影响，在研究用轴流压气机上进行了一系列的基础研究。这种高、低能非定常气动扰动力函数的激发原因有，周向进口流场畸变和叶型类障凝物引起的尾迹，典型的有叶型、支柱或探针激发的尾迹。

INTRODUCTION

Nonuniform inlet flow to a rotor represents the most common aerodynamic excitation source for aerodynamically forced vibrations. These nonuniformities can be broadly categorized as wake excitations or inlet distortions. These nonuniformities result in detrimental aeromechanical effects, with the distortion and wakes both representing unsteady aerodynamic forcing functions to downstream turbomachine blade rows.

Distortions and wakes are both high energy aerodynamic forcing functions which are characterized by low to moderate values of the reduced frequency. On a first principle basis, they are both analyzed by first defining the unsteady aerodynamic forcing function in terms of harmonics. The periodic of an airfoil row to each harmonic is then assumed to be comprised of two components. One is due to the harmonic components of the unsteady aerodynamic forcing function being swept past the nonresponding airfoil row, termed the streamwise and transverse gust responses. The second, the self-induced unsteady aerodynamics, arises when a vibrational response of the airfoil row is generated.

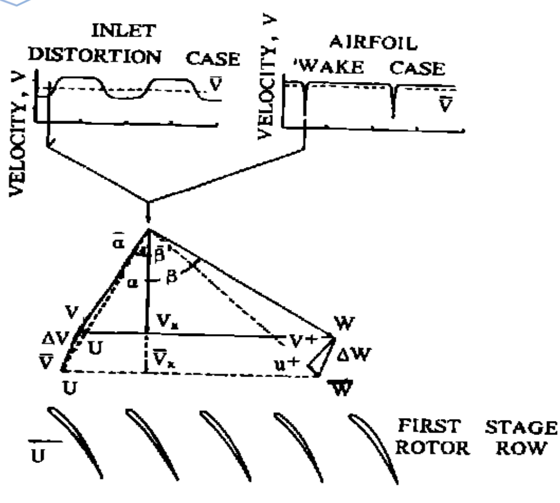

Figure 1. Forcing function decomposition

Current state-of-the-art unsteady aerodynamic models for the prediction of forced response do not consider differences in the various aerodynamic forcing functions. Also, the gust and motion-induced unsteady aerodynamic models involve many phyical and numerical assumptions.

This paper is received in January, 1990.

Therefore, experimental modeling of the fundamental distortion and wake generated blade row periodic unsteady aerodynamic response, including both the forcing function and the resulting blade row unsteady aerodynamics, is needed for validation and enhancement of theoretical and numerical models.

In this paper, the fundamental 2-E gust unsteady aerodynamic response of a multistage turbomachine blade row is experimentally investigated for the first time. This is accomplished by means of a series of experiments performed in an extensively instrumented axial flow research compressor. The 2-E unsteady aerodynamic forcing function excitations are generated by both a circumferential inlet flow distortion and the wakes from airfoil-type obstructions which are representative of an airfoil, strut, or probe excitation.

Two different two-per-rev aerodynamic forcing functions are considered (Figure 1): (1) the velocity deficit from two 90 degree circumferential inlet flow distortions and (2) the wakes from two upstream airfoil-type obstructions. These aerodynamic forcing functions to the first stage rotor blade row are measured with a rotating cross hot wire probe, with these data then analyzed to determine the streamwise and transverse unsteady velocity components, u^{+} and v^{+} shown in Figure 1. The resulting unsteady aerodynamic gust generated rotor blade surface unsteady pressure chordwise distributions are measured with embedded ultraminiature high response dynamic pressure transducers.

RESEARCH COMPRESSOR

The Purdue Axial Flow Research Compressor experimentally models the fundamental turbomachinery unsteady aerodynamic multistage interaction phenomena including the incidence angle, the velocity and pressure variations, the aerodynamic forcing function, the reduced frequency, and the unsteady blade row interactions. The compressor is driven by a 15 HP (11.19kW) DC electric motor and is operated at a speed of 2, 250 rpm. Each identical stage of the baseline compressor contains 43 rotor blades and 31 stator vanes having a British C4 profile, with the first stage rotor inlet flow field established by a row of 36 variable setting inlet guide vanes. The overall airfoil and compressor characteristics are: design flow rate—2.03kg/s; design axial velocity—24.4m/s; rotational speed—2250rpm; number of stages—2; stage pressure ratio—1.003; inlet tip diamter—420mm; hub/tip radius ratio—0.714; stage effciency—85%; aspect ratio, thickness/chord and chord C of all three are 2, 10 and 30mm respectively; others such as number of airfoil N, solidity C/S, camber θ and stagger angle λ are presented in Table 1.

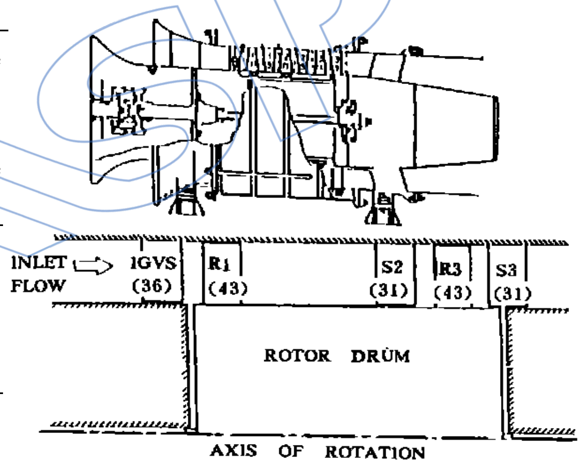

Figure 2. Research compressor comfiguration

Table 1. Overall airfoil and compressor characteristics

	N	*C/S*	θ	λ
ROTOR	43	1.14	27.95	36
STATOR	31	1.09	27.70	- 36.1
IGV	36	0.96	36.9	18.5

For these experiments, the first stage rotor blade row was extensively instrumented. Due to the large gap between the IGV row and the first stage rotor row, approximately 75% vane chord, the potential flow effects are negligible compared to the viscous wakes. To eliminate any potential flow effects from the downstream stator row on the instrumented first stage rotor blades, the first stage stators and second stage rotors were removed, as schematically depicted in Figure 2.

INSTRUMENTATION

Both steady and unsteady first stage rotor blade row data are required. The former quantify the rotor mean inlet flow field and midspan steady loading distribution. The latter define the periodic aerodynamic forcing function and the resulting midspan blalde surface periodic pressure distributions.

The inlet flow fields, both steady and unsteady, are measured with a rotating cross hot-wire probe mounted 30% of blade chord upstream of the rotor row. The probe is calibrated and linearized for velocities from 18.3m/sec to 53.4m/sec and +/- 35° angular variation, with the accuracy of the velocity magnitude and flow angle determined to be 4% and +/- 1.0 degree, respectively. Centrifugal loading effects on the rotating hot-wire sensor resistances and, thus, responses were found to be negligible.

The detailed steady aerodynamic loading on the rotor blade surfaces is measured with a chordwise distribution of 20 midspan static pressure taps, 10 on each surface. The static pressure at the rotor exit plane, measured with a rotor drum static tap, is used as the blade surface static pressure reference. These static pressure measurements are made using a rotor based 48 port constant speed drive Scanivalve system located in the rotor drum.

The measurement of the midspan rotor blade surface unsteady pressures is accomplished with 20 ultra-miniature, high response transducers embedded in the rotor blades at the same chordwise locations as the static pressure taps. To minimize the possibility of flow disturbances associated with the inability of the transducer diaphragm to exactly maintain the surface curvature of the blade, a reverse mounting technique is utilized. The pressure surface of one blade and the suction surface of the adjacent blade are instrumented, with transducers embedded in the nonmeasurement surface and connected to the measurement surface by a static tap. The embedded dynamic transducers were both statically and dynamically calibrated. The static calibrations showed good linearity and no discernible hysteresis. The dynamic calibrations demonstrated that the frequency response, in terms of gain attenuation and phase shift, were not affected by the reverse mounting technique. The accuracy of the unsteady pressure measurements, determined from the calibrations, is +/- 4%

The rotor based static pressure Scanivalve transducer, rotating hot-wire probe and 20 blade surface dynamic pressure transducers are interfaced to the stationary frame-of-reference through a 40 channel slip ring assembly. On-board signal conditioning of the transducer output signals is performed to maintain a good signal-to-noise ratio through the slip ring. The remaining 17 channels of the slip-ring assembly are used to provide excitation to the transducers and on/off switching excitations to the Scanivalve DC Motor.

DATA ACQUISTION AND ANALYSIS

STEADY DATA The rotor blade surface static pressure data, measured with the rotor-based Scanivalve system, are defined by a root-mean-square error analysis of 20 samples with a 95% confidence interval. The reference for these midspan blade pressure measurements is the static pressure at the exit of the rotor measured on the rotor drum. Thus, the blade surface and the reference static pressures are measured at different radii. Hence, a correction for the resulting difference in the radial acceleration is applied in calculating the balde surface static pressure coeffcient defined in Equation 1.

$$\overline{C}_p = (\overline{P}_s - \overline{P}_{exit}) / (1/2\rho U_t^2) \qquad (1)$$

where U_t is the rotor blade tip speed, $\overline{P}_s$ and $\overline{P}_{exit}$ *are rotor blade surface and drum steady pressures.*

PERIODIC DATA The periodic data of interest are the harmonic components of the aerodynamic forcing function to the first stage rotor blade row together with the resulting rotor blade surface unsteady pressure and unsteady pressure differences. These are determined by defining a digitized ensemble averaged unsteady aerodynamic data set consisting of the rotating cross hot-wire probe and blade surface dynamic pressure transducer signals at each steady operating point. In particular, these time-variant signals are digitized with a high speed A-D system at a rate of 20 kHz and then ensemble averaged. The key to this averaging technique is the ability to sample data at a preset time, accomplished by an optical encoder mounted on the rotor shaft. The microsecond range step voltage signal from the encoder is the data initiation time reference and triggers the high speed A-D multiplexer system. To significantly reduce the random fluctuations superimposed on the periodic signals of interest, 200 averages are used. A Fast Fourier Transform (FFT) algorithm is then applied to these ensemble averaged signals to determine the harmomic components of the unsteady aerodynamic forcing function and the resulting rotor blade surface harmonic unsteady pressures and pressure differences.

The unsteady inlet flow field to the rotor row, measured with the rotating cross hot-wire probe, is quantified by the inlet relative velocity and flow angle. The velocity triangle relations depicted in Figure 1 are then used to determine the detailed unsteady velociity into the rotor row, in particular, the streamwise and transverse velocity components, u^+ and v^+ respectively. These are then Fourier decomposed to determine their harmonic components, u_i^+ and v_i^+.

The various unsteady aerodynamic gust mathematical models reference the gust generated airfoil aerodynamic response to a transverse gust at the leading edge of the airfoil. However, in the experiments the time-variant data are referenced to the initiation of the data acquisition shaft trigger pulse. Thus, for consistency with the models, the periodic data are further analyzed and referenced to a transverse gust at the leading edge of the first stage rotor blade. This is accomplished by assuming that: (1) the aerodynamic forcing function remains fixed in the stationary reference frame; and (2) the forcing function does not change from the probe axial location to the rotor row leading edge plane.

The rotor blade surface unsteady pressure data, measured with the embedded high response pressure transducers, are analyzed to determine the harmonics of the chordwise distribution of the unsteady pressure coefficient, $C_{\Delta pi}$, and the unsteady pressure difference coefficient, $C_{\Delta pi}$. These are defined in Equation 2 and are specified from the Fourier coeffcients of the digitized unsteady pressure transducer signals. Thus, the final form of the gust generated rotor blade row unsteady aerodynamcis is the chordwise distribution of the harmonic complex unsteady pressure and pressure difference coeffcients $\hat{C}_{\Delta pi}$.

$$\hat{C}_{pi} = p_i / [\rho \bar{V}_x^2 (v_i^+ / \bar{V}_x) \bar{\beta}] , \quad C_{\Delta pi} = C_{pi,pressure} - C_{pi,suction} \tag{2}$$

where p_i is the harmonic unsteady pressure, $\bar{V}_x$ is the mean axial velocity, and $\bar{\beta}$ is the relative mean flow angle, C_{pi} is rotor blade harmonic unsteady pressure coefficient.

RESULTS

A series of experiments are performed to investigate and quantify the effects of different aerodynamic forcing functions on periodic 2-E gust unsteady aerodynamics of a first stage rotor blade row. 2-E unsteady aerodynamic forcing function excitations are generated by a circumferential inlet flow distortion and the wakes from airfoil-type obstructions. In these experiments, the two two-per-rev forcing functions are equivalent in terms of aerodynamically forced response as each has approximately the same nominal value for the first harmonic streamwise-to-transverse gust amplitude ratio.

1. **PERIODIC AERODYNAMIC FORCING FUNCTIONS** The Fourier decomposition of the inlet distortion and wake aerodynamic forcing functions to the first stage rotor in terms of the gust components are presented in Figures 3 and 4. The inlet distortion results in a dominant two-per-rev excitation with smaller higher harmonics. With the wake forcing function, a strong two-per-rev signal is again present. However, the higher harmonic amplitudes are approximately the same magnitude as the generating wake two-per-rev fundamental for the streamwise gust components and are larger for the transverse gust component.

2. **BLADE SURFACE STATIC PRESSURES** The effect of steady aerodynamic loading, characterized by the mean incidence angle, on the rotor blade surface static pressure coeffcient for both the inlet distortion and the obstruction wake forcing function are shown in Figure 5. The level of steady loading only affects the static pressure distribution on the perssure surface over the front 40% of the chord. On the suction surface, the steady loading variation has a large effect on the static pressure distribution over the entire suction surface. Also, these data exhibit no indication of flow separation. Of particular interest to the unsteady experiments, these data clearly show that these different aerodynamic forcing functions have no effect on the steady aerodynamic performance of the rotor, i. e., the airfoil

steady surface static pressures are independent of the unsteady aerodynamic forcing function.

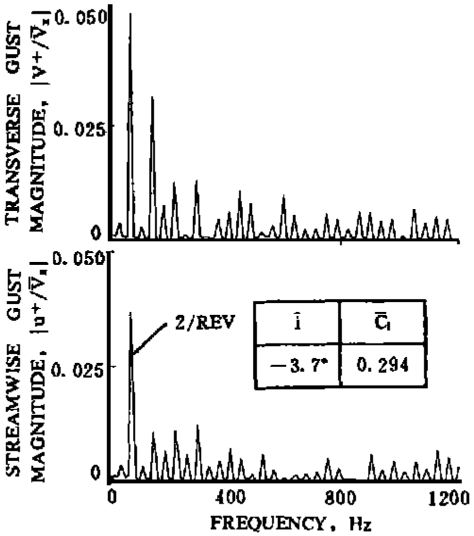

Figure 3. Fourier decomposition of inlet distortion forcing function

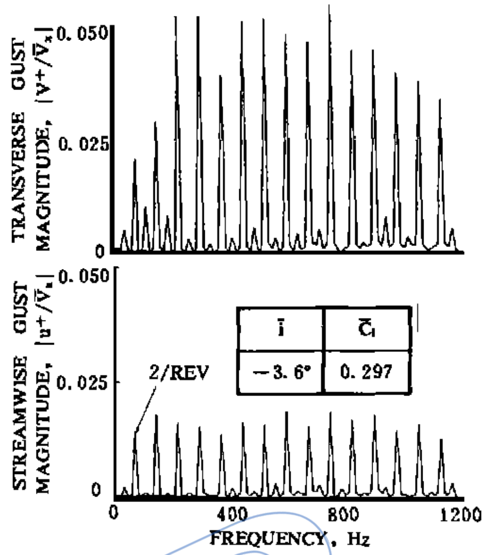

Figure 4. Fourier decomposition of wake forcing function

3. **ROTOR ROW PERIODIC AERODYNAMIC RESPONSE** The periodic aerodynamic first

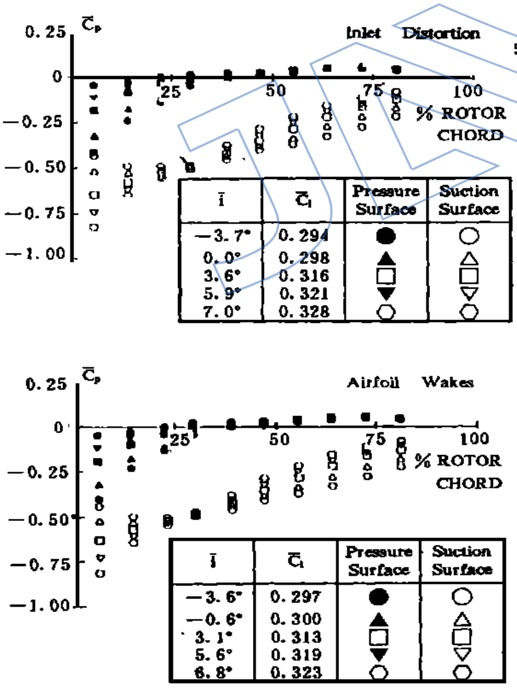

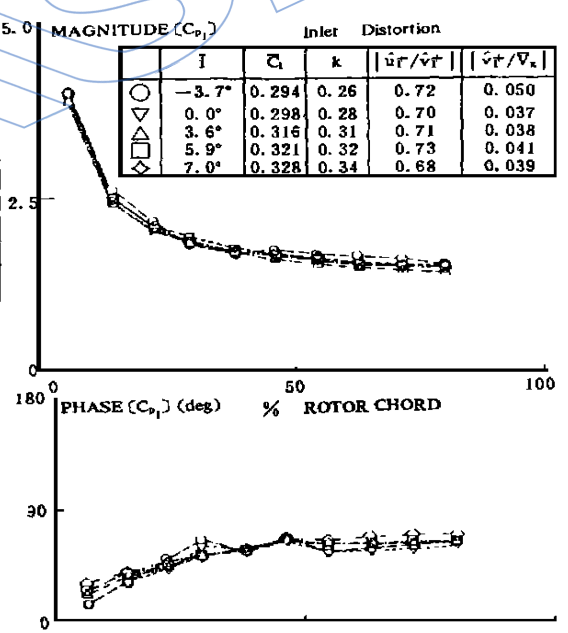

Figure 5. Forcing function and steady loading effects on $\bar{C}_p$ Figure 6. Pressure surface steady loading effect on C_{p1}

harmonic response of the first stage rotor blade row to the inlet distortion and wake forcing functions, including the effect of steady aerodynamic loading, are presented in Figures 6, 7 and 8. In particular, these figures present the chordwise distributions of the complex unsteady pressure coefficient on the individual rotor blade surfaces as well as the corresponding complex unsteady pressure difference coefficients generated by the inlet distortion first harmonic two-per-rev aerodynamic forcing function.

(1) **Pressure Surface Unsteady Pressures** The effect of steady aerodynamic loading level on the first harmonic of the complex unsteady pressure distribution on the rotor blade pressure surface for the inlet distortion is shown in Figure 6. The unsteady pressure magnitude data decrease monotonically with increasing chord for all steady loading levels. Also, this form of the dimensionless unsteady pressure coefficient, (Eq. 2) results in the compression of these magnitude data for all mean flow incidence angle values. Thus, the magnitude of the unsteady pressure response on the blade pressure surface, i. e., the low camber airfoil surface, is primarily due to the level of steady loading as characterized by the mean flow incidence angle. With regard to the unsteady pressure phase data on this airfoil surface, they increase over the front half of the chord and are independent of the level of steady loading.

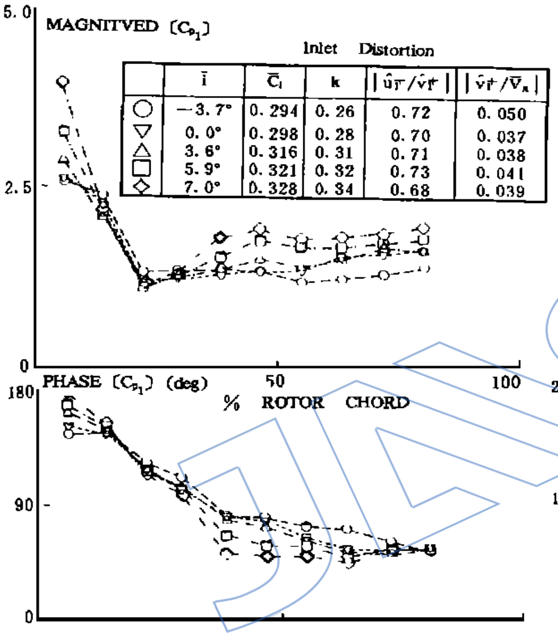

Figure 7. Suction surface steady loading effect on C_{p1}

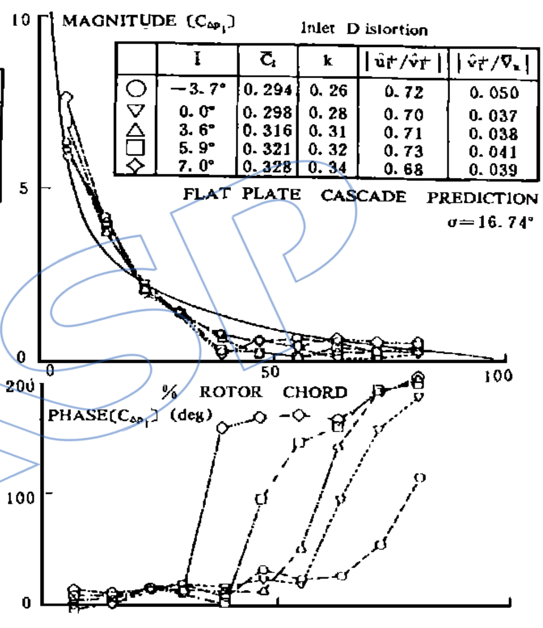

Figure 8. Steady loading effect on $C_{\Delta p_1}$

(2) **Suction Surface Unsteady Pressures** The effect of steady aerodynamic loading on the first harmonic complex unsteady pressure on the rotor blade suction surface is shown in Figure 7 for the inlet distortion. In contrast to the pressure surface, the form of the dimensionless unsteady pressure coefficient, Equation 2a, does not compress the suction surface magnitude data with mean flow incidence angle, the exception being between 13% and 20% of the chord for the inlet distortion. The unsteady pressure magnitude data decrease to a minimum and then increase as the chord is traversed. Also, these magnitude data are dependent on the steady loading, increasing with increased steady loading. The corresponding phase data decrease over the chord, in the leading edge and mid-chord regions, are dependent on the steady loading. Near the leading edge, increased loading results in an increase in the phase whereas in the mid-chord region the phase decrease in value.

(3) **Unsteady Pressure Differences** The effect of steady loading on the first harmonic complex unsteady pressure difference across the rotor blade is shown for the inlet distortion forcing function in Figure 8. Also presented as a reference are the flat plate cascade predictions. The magnitude data generally decrease with increasing chord, in trendwise agreement with the predictions. Also, these magnitude data increase with increasing steady

loading. The corresponding unsteady pressure difference phase data are nearly constant and independent of the level of steady loading in the front chord region. There is a sharp increase in the phase data in the mid to aft chord regions of the airfoil, with the onset location of this sharp increase moving towards the leading edge with increasing mean flow incidence angle.

SUMMARY AND CONCLUSION

The fundamental 2-E gust unsteady aerodynamic response of a multistage turbomachine blade row has been experimentally investigated for the first time. General experimental results are noted:

1. The inlet distortion forcing function shows a dominant two-per-rev, with much smaller higher harmonic content. In contrast, the wake forcing function shows a strong two-per-rev with higher harmonics of larger amplitudes

2. The rotor steady aerodynamic performance is independent of the forcing function.

3. On the pressure surface, the inlet distortion generated unsteady pressure magnitude data decrease monotonically with chord and are compressed with respect to the mean flow incidence angle. The phase data increase over the front half of the chord and are independent of the steady loading level.

4. On the suction surface, the inlet distortion generated unsteady pressure magnitude data decrease to a minimum and then increase with chord. Also, they depend on the steady loading, increasing with increased steady loading. The phase data decrease over the chord and depend on the steady loading.

5. With regard to the inlet distortion generated unsteady pressure difference data, the magnitude data decrease with increasing chord and increase with increased incidence angle. The phase data are nearly constant and indepentent of the loading in the front chord region. A sharp increase in phase in the midchord region, with the onset location moving forward with increasing incidence angle.

ACKNOWLEDGEMENTS Research sponsored by the Air Force Office of Scientific Research (AFSC) under Contract F49620-88-C-0022. The United States Government is authorized to reproduce and distribute reprints for governmental purposes notwithstanding any copyright notation hereon.

REFERENCES

[1] Capece, V. R., Manwaring, S. R., and Fleeter, S., "Unsteady Blade Row Interactions in a Multi-Stage Compressor" AIAA Journal of Propulsion and Power, Vol. 2, No. 2, 1986.

[2] Capece, V. R., and Fleeter, S., "Unsteady Aerodynamic Interactions in a Multi-Stage Compressor", ASME Journal of Turbomachinery, Vol. 109, No. 3, 1987.

[3] atko Jr., F. T. and O' Hara, J. A., "The Aeromechanical Response of an Advanced Transonic Compressor to Inlet Distortion", ASME Paper 87-GT-189, 1987.

[4] Fleeter, S., Jay, R. L., and Bennett, W. A., "Rotor Wake Generated Unsteady Aerodynamic Response of a Compressor Stator", ASME Journal of Engineering for Power, Vol. 110, o. 4, 1987.

[5] Fleeter, S., Bennett, W. A., and Jay, . L., "The Time Variant Aerodynamic Response of a Stator Row Including the Effects of Airfoil Camber", ASME Journal of Engineering for Power, Vol. 102, No. 2, 1980.

[6] Gallus, H. E., Lambertz, J., and Wallman, Th., "Blade-Row Interaction in an Axial-Flow Subsonic Compressor Stage", ASME Journal of Engineering for Power, Vol. 102, No. 1, 1980.

[7] Smith, S. N., "Discrete Frequency Sound Generation in Axial Flwo Turbomachines", ARC R&M 3709, 1971.